Clays and Clay Minerals, Vol. 55, No. 2, 189–199, 2007.

ROLE OF SMECTITE IN SILICEOUS-SINTER FORMATION AND MICROBIAL-TEXTURE PRESERVATION: OCTOPUS SPRING, YELLOWSTONE NATIONAL PARK, WYOMING, USA

JENNIFER E. KYLE AND PAUL A. SCHROEDER*

Department of Geology, University of Georgia, Athens, GA, 30602-5201, USA

Abstract—A siliceous sinter collected from Octopus Spring in Yellowstone National Park, USA contains an occluded volcanic rock fragment that has undergone alteration. The sinter piece beyond the fragment is mostly dominated by opal-A with trace amounts of bacterial cells, calcite and detrital quartz. Within the altered rock region, the mineral assemblage is dominated by dioctahedral smectite and quartz with trace amounts of pseudobrookite, ilmenite, rutile and hematite. Onset of opal-CT formation was only found in the outer spicular region of the sinter, which is unexpected given that this outer part represents newest growth. A reaction mechanism is proposed whereby the alteration of feldspar to smectitic clay locally produces excess silica, and alkali metal, and raises pH. As the clay mineral forms, it sequesters ions from pore fluids thereby inhibiting the opal-A phase change to more ordered opal-CT. Ions such as Mg are known to promote the opal-A to opal-CT reaction. Smectite formation therefore may assist microbial-texture preservation processes as excess silica produced increases the rate at which primary opal-A is formed. The altered zone also retains the greatest amount of fixed C and fixed N (operationally defined as C and N retained upon combustion at 450ºC). The fixed N probably represents ammonium trapped in the exchangeable interlayer site of the smectite. This fixed N may serve as a potential biological signature of microbial activity in ancient rocks formed in similar environments.

Key Words—Biosignatures, Clays, Montmorillonite, Nitrogen, Opal, Pseudobrookite, Siliceous Sinter, Yellowstone National Park.

INTRODUCTION

Siliceous sinters formed in terrestrial hot springs under high temperature (75−100ºC), reducing, and silica-saturated conditions and are thought to be formed in conditions similar to that of early Earth (Konhauser *et al*., 2003; Lynne *et al*., 2006). Sinters are of interest because they contain active sites of microbial activity and biomineralization. The transition from disordered opal-A ($SiO_2 \cdot nH_2O$) to more ordered forms (*e.g.* opal-C, opal-T, opal-CT, quartz and moganite) can affect the preservation potential of microbes such as hyperthermophilic *Aquifex* and *Thermotoga*, which are known to live in modern environments (Blank *et al.*, 2002). Understanding the mineralogical transformations of sinters and microbial silicification and preservation is important for interpreting the ancient rock record where similar fabrics are found (Rimstidt and Cole 1983; Rice *et al.*, 1995; Cady and Farmer, 1996; Westall *et al.*, 1995; Renaut *et al.*, 1998; Herdianita *et al.*, 2000; Jones *et al.*, 2001, 2003; Konhauser *et al.*, 2004; Lynne and Campbell, 2004; Pancost *et al.*, 2005). The geochemical environment and rate of diagenetic opal transformation are two important factors in controlling the preservation of microbial forms and their isotopic/organic chemical composition (Lynne *et al.*, 2006).

Siliceous sinters typically form in spring fluids supersaturated with respect to amorphous silica (they can also form from evaporating near-saturated spring fluids). Opal-A formation begins by nucleation in a colloidal suspension that then deposits out of solution (Rimstidt and Cole, 1983). Microbial cells often act as site templates for opal-A nucleation and subsequent sinter formation can then continue due to the lower surface energy barrier towards precipitation. As microbial cells become silicified, a morphological and/or chemical signature may be preserved within the sinter (Cady and Farmer, 1996). Morphological preservation is sometimes reduced as opal-A undergoes dissolution and precipitation reactions form more ordered silica phases. The potential effects that clay minerals have in the formation and preservation of microbial signatures in terrestrial hot springs is not well documented.

In October of 2001, an opportunity was afforded to collect a clay-rich siliceous sinter deposit from the rim of the Octopus Spring vent (Figure 1) in Yellowstone National Park (YNP), Wyoming. The purpose of the collection was to look at micrometer-scale endolithic microbe-mineral relationships. The highly restricted and regulated nature of sampling within YNP makes extensive surveying of active vent mineralogy in YNP nearly impossible. Although sampling was limited, the intent was to characterize endolithic microbial forms and mineral crystal chemistry using high-resolution miner-

* E-mail address of corresponding author:
schroe@uga.edu
DOI: 10.1346/CCMN.2007.0550208

Figure 1. Octopus Spring, YNP sample location. Arrow indicates collection site.

alogical, textural, and chemical methods. The purpose of this paper is to report on sinter mineralogy and the potential effects of co-existing clay minerals on opal-A transformation and the role that clays may play in preserving biological and chemical signatures in ancient terrestrial hot springs found in the rock record.

Site description

Octopus Spring is a gently surging, non-boiling (Braunstein and Lowe, 2001), near-neutral, alkali chloride hot spring that is fed from an aquifer with a subsurface temperature >175ºC (Fournier and Rowe, 1966; Hinman and Lindstrom, 1996; Ball *et al.*, 1998; McCleskey *et al.*, 2004). The near-surface temperature of the pool varies from slightly more than 93ºC over the vent to <73ºC in shallow pools away from the vent (Braunstein and Lowe, 2001). Small surge cycles of 4–5 min with 2 to 3 cm of water level fluctuations do not cause rim overflow of the spring (Braunstein and Lowe, 2001). A siliceous sinter deposit was collected next to the vent where high-temperature waters were emerging (Figure 1). The surface of the deposit collected was flat, lily pad in shape, with a thin green microbial mat forming along the upper side of the sinter. Under the microbial mat, spicules formed, becoming longer towards the bottom of the deposit and protruding towards the spring. The morphology of the sinter is similar to others found around the vent (see Lowe and Braunstein, 2003, for example).

During the past 2.7 Ga of the recorded geological history of YNP, the region has undergone three explosive rhyolitic eruptions dated at 2.0, 1.3 and 0.6 Ga (Fritz, 1985). The stratigraphy of the Lower Geyser Basin (where Octopus Spring is located) consists of siliceous sinter material at the surface, sinter with interbedded travertine and hydrothermally altered detrital sediment up to 10 m below the surface, glacial sediments with interlayered tuff at 10–32 m, and then rhyolitic lavas at depths of >32 m (Bargar and Beeson, 1981). Currently, a mantle plume 5 to 6 km beneath YNP is causing uplift at a rate of 2.5 cm/y as molten rock moves towards the surface (Fritz, 1985).

METHODS

A siliceous sinter deposit, ~7 cm × 5 cm, was collected from the edge of the Octopus Spring vent (Figure 1). Initial procedures involved cutting cross-sections of the sinter with a diamond-blade saw. Five internal textural zones were identified based on visual examination of the cross-sections (Figure 2). These

Figure 2. Siliceous sinter collected from Octopus Spring. The thinly laminated crust is underlain by a green microbial mat. Image of sinter shown protrudes into the spring.

https://doi.org/10.1346/CCMN.2007.0550208 Published online by Cambridge University Press

zones are herein described as (1) a crustal region (containing fine laminations), (2) an altered region (devoid of texture), (3) a dark/light laminated region (composed of thin dark and light laminations), (4) a dark laminated region (containing convex-up laminations), and (5) a spicular region.

The textural morphology of the sinter was examined using a thick section (~100 μm) that was prepared for backscatter electron imaging (JEOL 8600 electron probe; accelerating voltage of 15 kV) and confocal laser scanning microscopy (CLSM; Bio-Rad MRC 600; Argon laser wavelength of 543 nm). Standard thin-sections (30 μm) were examined under a light microscope in which images were taken in plane-polarized light using a Nikon CoolPix 990 camera mounted on an Olympus BX40 light microscope. Scanning electron microscopy (SEM) was used to study textural morphologies and microbial remnants on the micrometer scale. Freshly fractured sinter surfaces from each zone were mounted onto aluminum SEM stubs with carbon paste and then carbon coated. The images were taken at 3.0 kV on a field emission Leo 982 microscope.

Mineralogical and chemical analyses were conducted using X-ray diffraction (XRD; Scintag XDS 2000), Electron microprobe (JEOL 8600), and a Micro-Dumas combustion furnace (NA 1500 C/H/N). Samples were collected from each zone by micro-drilling and then ground using a mortar and pestle. Samples for XRD analysis were applied to a zero-background quartz plate using acetone slurries to achieve random particle orientation and to eliminate substrate scatter. Experimental XRD parameters included CoKα radiation, 2º/4º scattering slits and 0.5º/0.3º receiving slits, 0.02º step, and a scan rate of 10 s per step. Oriented mounts of material from the altered zone were prepared by Ca, K and Mg saturation under ethylene glycol saturation (Moore and Reynolds, 1997) and scanned at a rate of 1º per second. A random-mount XRD scan of the 060 reflections from clays in the altered zone was also conducted to distinguish the dioctahedral (~1.50 Å) and trioctahedral (~1.53 Å) nature of the clay minerals. Trace-element data were collected on the JEOL electron microprobe using wavelength dispersive spectroscopy (WDS). Data were collected along points on a transect ranging from the crust to the base of the dark zone on polished thick sections. Point selection was based on the appearance of dark and light laminae and regions around pores.

Carbon and nitrogen Micro-Dumas combustion analysis employed ~15 mg of ground sample encapsulated into tin foil. A second set of samples was placed into silver capsules, heated at 450ºC overnight, and subsequently analyzed for carbon and nitrogen (Schroeder and Ingall, 1994). Comparison of carbon and nitrogen values from combusted and non-combusted samples allows for an assessment of organic *vs.* inorganic association of the two elements (Schroeder and McLain, 1998).

RESULTS

Mineralogy

X-ray diffraction analysis of material from each of the five internal zones revealed a broad region of semi-coherent scatter typical of opal-A with maximum intensity centered at 4.03 Å (Figure 4a) for all zones. The onset of opal-CT formation (identified by both opal-A with ordered opal-CT beginning to form; Lynne and Campbell, 2004) was only identified in the spicular zone, where diagnostic XRD peaks of 4.11 Å and 2.51 Å appear. The altered interior differed from the other zones by the presence of dioctahedral smectite and the greatest abundance of quartz. This clay-rich region resides within the center of the deposit and is surrounded by laminated opal-A. Visual inspection of the altered zone revealed embedded, dark, millimeter-sized, roughly spherical, grains. X-ray diffraction analysis indicates that these dark grains were composed of pseudobrookite (Fe_2TiO_5) and hematite (Figure 4b). Microprobe analysis of the dark grains revealed elements consistent with pseudobrookite, as well as hematite, rutile and ilmenite. The XRD analysis also revealed minor calcite in the crust, altered interior, and the dark laminated zones.

Cation saturation of the smectite with Ca, Mg and K and ethylene glycol solvation results in d_{001} peaks at 17.2, 15.6 and 16.4 Å, respectively. Forward modeling with Newmod® (Reynolds, 1980) found visual best-fits using parameters for a randomly interstratified vermiculite-smectite. Observed patterns for Ca-, Mg- and K-saturated samples agree well with model patterns having 99%, 25% and 45% smectite-like layers (Figure 5). The highest degree of layer collapse occurs with Mg saturation, which suggests a heterogeneous layer-charge distribution. Mg^{2+} ions possess the largest charge-to-mass ratio amongst the three cations (*i.e.* for Ca^{2+}, Mg^{2+} and K^{+} = 0.22, 0.29 and 0.16, respectively, where z = charge and m = mass). Collapse of layers in

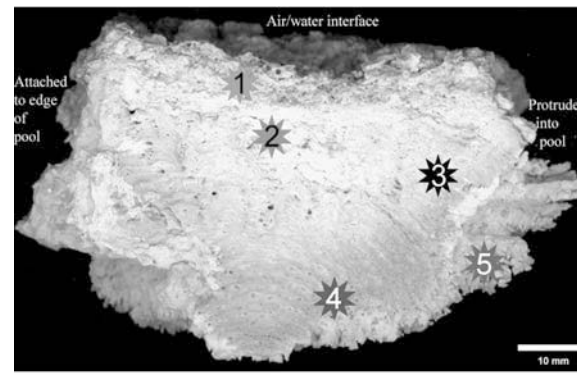

Figure 3. Cross-section of the sinter. The left side of the deposit was attached to the rim of the pool, whereas the right side protruded into the spring. The sinter was divided into five zones: (1) crustal, (2) altered, (3) dark/light laminated, (4) dark laminated, and (5) spicular.

https://doi.org/10.1346/CCMN.2007.0550208 Published online by Cambridge University Press

the presence of a small, high-charge interlayer cation suggests some negative layer charge is derived from the octahedral sheet (MacEwan and Wilson, 1980). The collapse of layers with K saturation (although to a lesser extent than Mg saturation) also supports the idea of heterogeneous layer charges. Collapse in the presence of K^+ indicates that some negative charge may be from the tetrahedral-sheet substitution of Al for Si. Of the three cations, Ca^{2+}, Mg^{2+} and K^+ (with ionic radii of 0.99, 0.65 and 1.33 Å, respectively), K^+ fits best into the ditrigonal cavity of silica sheets (Bailey, 1984). The important result here is that this smectite contains many interlayer sites whose compensating charges are high enough to retain trace levels of cations such as NH_4^+, which may be produced in the surrounding system (discussed below).

Chemical constituents and trace-element chemistry

Whole-rock analysis for C and N reveal weight percent values that range from 0.33 to 0.76 and 0.03 to 0.08, respectively (Table 1). Samples heated to 450ºC have measured C and N weight percent values that range from 0.11 to 0.38 and 0.031 to 0.034, respectively.

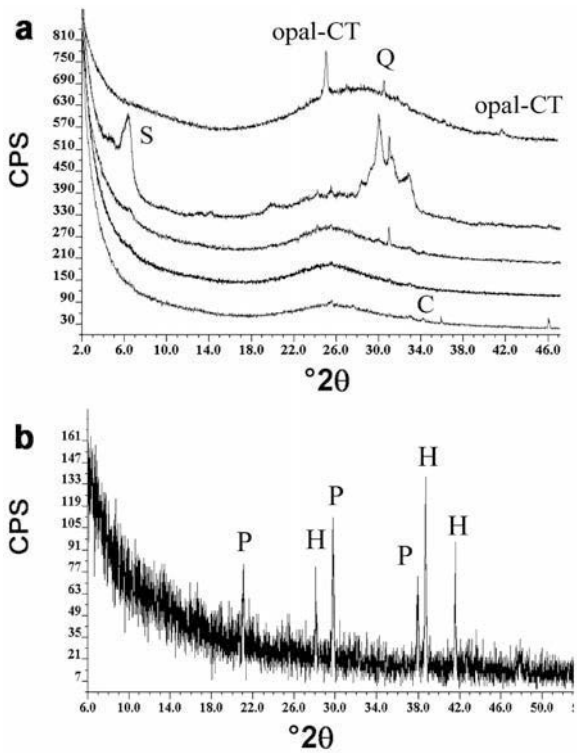

Figure 4. XRD patterns of sinter from each zone: (a) opal-A is represented by the broad central peak around 25º2θ or 4.03 Å. The upper pattern is of the spicular zone, then altered, crustal, dark/light laminated, and dark laminated at the bottom. Opal-CT, smectite (S), quartz (Q), and calcite (C) were also identified. (b) Dark mm-sized grains of pyrite (P) and hematite (H) found within the altered zone. CoKα radiation.

Directly comparing differences in weight percents before and after heating is biased by weight losses associated with dehydroxylation of clay minerals and opal. Thermogravimetric analysis (TGA) revealed that all samples yielded similar weight losses over the heating ranges of 25–300ºC, 300–550ºC, and 550–900ºC, with average weight percent losses for these ranges of 6%, 2% and 1.5%, respectively. The shapes of the TGA curves and their differentials (data not shown) are typical for smectite, organics, and opal-A, with endotherms in region of 120ºC (smectite dehydration), 200ºC (opal-A dehydration), 380ºC (organic oxidation), and 600ºC (smectite dehydroxylation) (Herdianita *et al.*, 2000; Guggenheim and Koster van Groos, 2001). The WDS analysis revealed that the altered interior contains the smallest amount of Si, and the greatest concentration of the trace elements Al, Mg and Ca. The presence of calcite from the dark/light zone was also detected by CLSM, where it appears as a naturally fluorescent material, coating pore spaces in no distinct pattern (Figure 6).

Textural morphologies

Of the five textural zones identified in this study (crust, altered, dark/light laminated, dark laminated and spicular), four were identified by Lowe and Braunstein (2003), who also studied sinter from Octopus Spring. The structureless, clay-rich region (altered zone) was not documented in Braunstein and Lowe (2001) or Lowe and Braunstein (2003) leading us to believe that this zone may be unique to this sample (additional collection of sinter to determine the frequency of clay-rich zones was not permitted by YNP authorities). The cross-section of the sinter reveals that the top of the sinter changes from very fine linear laminations to wavy laminations (*i.e.* stromatolitic texture) throughout the middle of the sinter, except in the altered zone, which is structureless. Laminations continue to alter into convex-up lamina-

Table 1. Total wt.% C and N values for siliceous sinter from Octopus Spring, YNP.

Sinter zone	Total C (%)	Total N (%)	C/N ratio
Unheated			
Crust	0.71	0.075	9.41
Altered	0.43	0.035	12.3
Dark/light laminated	0.67	0.047	14.3
Dark laminated	0.76	0.069	11.1
Spicular	0.33	0.069	4.70
After heating to 450ºC			
Crust	0.13	0.034	3.95
Altered	0.38	0.031	12.3
Dark/light laminated	0.12	0.031	3.94
Dark laminated	0.13	0.033	3.97
Spicular	0.11	0.031	3.59

https://doi.org/10.1346/CCMN.2007.0550208 Published online by Cambridge University Press

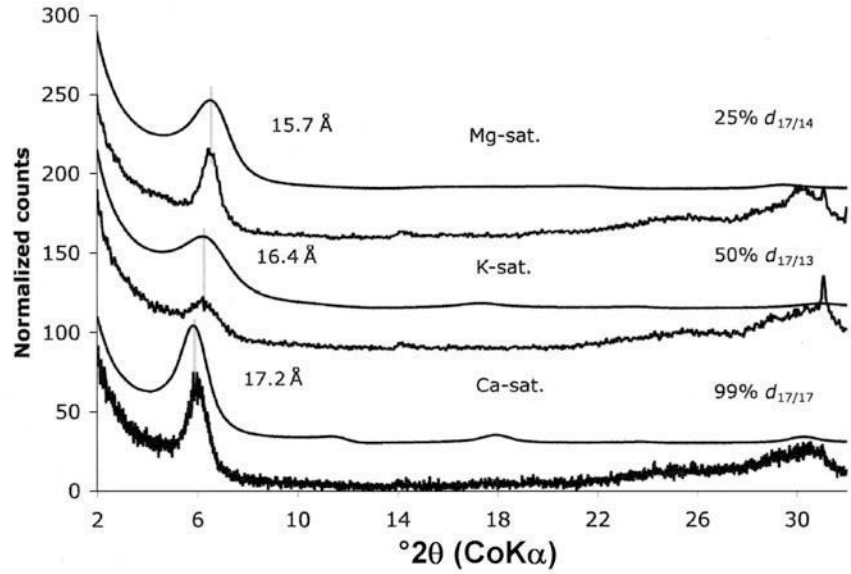

Figure 5. XRD of cation-saturated clays from sinter alteration zone (solid lines). Modeled patterns (smooth lines) for random mixed-layering using a 17.2 Å dioctahedral layer type for the first layer (Reynolds, 1980). Ca-, K- and Mg-saturated simulations, respectively, used a 17.2 Å 2-ethylene glycol layer type for Ca, a 12.9 Å 1-ethylene glycol layer type for K, and a 14.3 Å vermiculite-like layer type for Mg. Percentages of expandable layers (17.2 Å) giving the best visual fit are shown in the figure. Vertical lines connecting peak maxima are placed to visually aid fit of both model and observed data sets. CoKα radiation.

tions near the bottom of the sinter with ooid-like structures, representing cross-sections of the spicules (Figure 7), found between the laminations (Figure 3). The spicular zone is also finely laminated and represents newest growth regions and is therefore the youngest part of the sinter. As this part of the spring does not experience rim overflow, sinter growth occurs laterally forming the lily-pad surface morphology commonly associated with this deposit (Lowe and Braunstein, 2003).

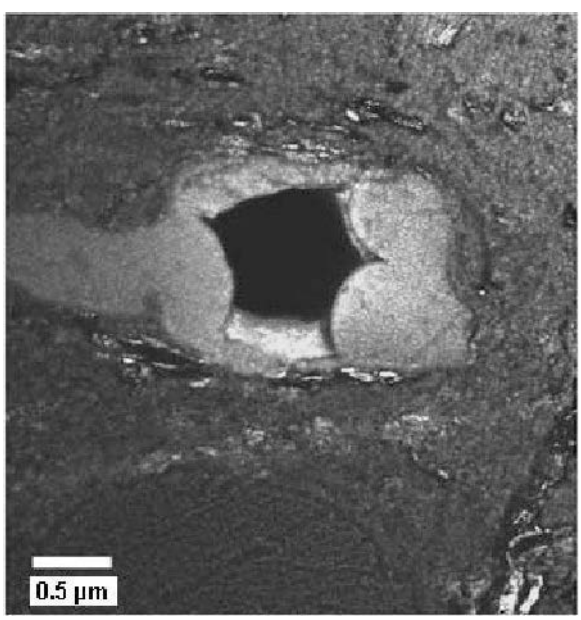

Figure 6. CSLM image of calcite- (light gray color) coated pore found in the dark laminated zone.

Natural cracks and fractures were abundant throughout the thin-section of the dark laminated zone (Figure 7a,b). Fractures radiate from the center of the concentric bands (Figure 7a,b). These radial cracks appear to be related to a desiccation that is a volume-loss event, perhaps related to opal-A diagenesis. A honeycomb structure with depressions roughly the size of opal-A spheres are noted in the crustal zone (Figure 8a). The altered zone contains occasional segmented filaments (Figure 8b). The dark zone is composed of very fine laminations that occasionally bear individual opal-A spheres ~0.7 µm in diameter and rod-shaped cells (Figure 8c,f). Vitreous coatings of opal-A cover prior precipitates of opal-A in the dark/light zone (Figure 8d). Amygdaloidal aggregates of opal-CT were not found in any of the zones. Figure 8e is a backscattered electron (BSE) image that shows the presence of filaments resembling microbial forms within the sinter pores. The microbial forms intertwined around each other within a pore space in the dark laminated zone. Randomly distributed silicified, microbe-like structures were found in all zones except the crust. The altered interior contained a silicified filament, ~30 µm long with evenly spaced segments (Figure 8b). Larger filamentous microbe-like structures, (~90 µm long) with a rough exterior are found in the dark laminated zone without the appearance of segmentation. Smooth rod-shaped microbial-like structures attached to the sinter substrate were found in the altered zone (Figure 8c).

https://doi.org/10.1346/CCMN.2007.0550208 Published online by Cambridge University Press

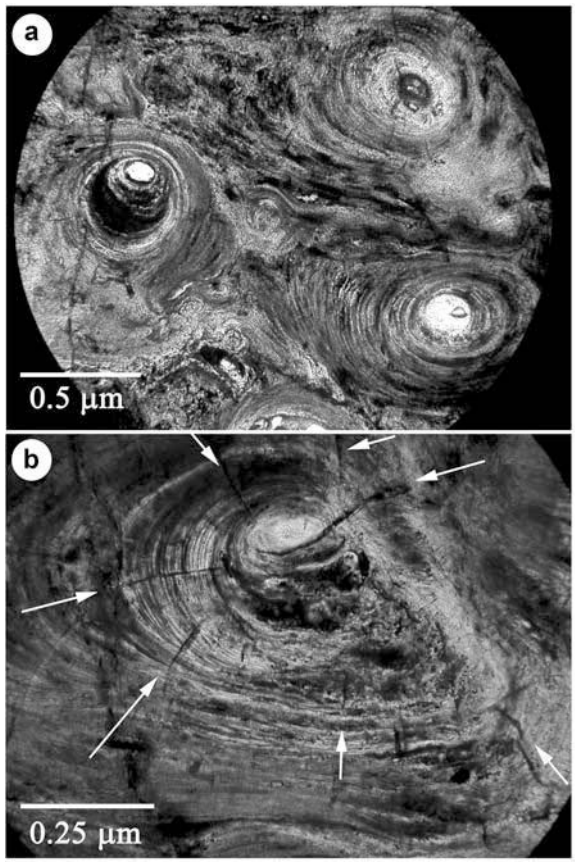

Figure 7. Light microscope images of dark laminated region. (a) Ooid-like structures. Note the cracks radiating through the concentric laminations in the left and top ooid-like structures. (b) Radiating cracks (noted by white arrows) from center of concentric laminations.

DISCUSSION

Role of smectite in opal-A to opal-CT phase transformation

The opal-A to opal-CT silica phase change is generally agreed to be a dissolution-precipitation reaction that is kinetically controlled by increasing temperature (Murata and Larson, 1975). Increasing crystal ordering marks this phase change along with decreasing water content and pore space, and increasing density (Rice *et al.*, 1995). Kastner *et al.* (1977) observed, in marine sedimentary environments, that the diagenesis of siliceous oozes from opal-A to opal-CT was inhibited by the presence of montmorillonite, but not in the presence of carbonate-rich sediments. Kastner *et al.* (1977) proposed that one important factor for opal-CT formation is the presence of Mg ions, which catalyze nucleation sites for opal-CT growth. When clays with exchangeable sites are present, such as montmorillonite, they sequester the Mg ions, thus delaying opal-CT formation. The mechanism for this inhibitory effect is ascribed to the idea that Mg was preferentially taken up by the montmorillonite. Kastner *et al.* (1977) also demonstrated experimentally that the diagenesis of siliceous oozes from opal-A to opal-CT was reduced in the presence of montmorillonite, but not in the presence of carbonate-rich sediments. The opal-A to opal-CT dissolution/precipitation reaction in marine settings is therefore promoted by the absence of smectitic clays.

Kastner *et al.* (1977) found greater amounts of opal-CT in carbonate-rich sediments, although carbonates generally do not affect the rate of silica diagenesis (Isaacs, 1982). In the Monterey Formation of California, calcite only influenced the kinetics of silica phase transformations when the silica concentration is eight times more abundant than detrital material present within the rock (Isaacs, 1982).

In accordance with the Kastner *et al.* (1977) theory, the smectite-dominated region of sinter should inhibit the rate of opal-A to opal-CT phase change. The Mg ion concentration within Octopus Spring is ~0.01 mg/L (McCleskey *et al.*, 2004). The porous nature of the sinter allows the clay to sequester cations from the passing pore fluids, thus reducing rates of opal-A to opal-CT phase change in the altered region relative to the other regions of the sinter. The spicule zone is less porous than the remaining zones and distal to the altered interior. It is proposed under this scenario that the spicule zone receives a continual supply of Mg ions from the hot spring thus enabling the onset of opal-CT formation. The appearance of clay minerals in sinter deposits is not common, although Mg-containing clays have been noted coating silica substrates and silicified microbes, and filling microbial molds (Jones *et al.*, 2003). No opal-CT was noted in Jones *et al.*, (2003) but the sinter was very young. The Kastner *et al.* (1977) observations are valid in relatively closed systems, which is not the case for the typically open system of a terrestrial hot spring. The spicular region of the sinter is continually provided with a new fluid source and experiences occasional dehydration during spring surging. The interior of the sinter, where hydrolysis and redox reactions are taking place within the rhyolitic fragment, is assumed to behave as a less open system where the kinetics of opal-A transformation are inhibited. Diffusion of water and ions in montmorillonite at temperatures of 60ºC is as much as five times slower than that of clay-free (*i.e.* water only) environments (Yoshito, 2002).

It is hypothesized that the clay-bearing altered zone in the sinter from Octopus Spring is the result of chemical weathering of a rhyolitic rock fragment. The inclusion of the rhyolitic rock into the sinter is not unlikely, given that the surrounding rocks are volcanic. This volcanic fragment would originally have been composed of quartz, feldspar (since altered to dioctahedral smectite), and pseudobrookite (since altered to hematite, ilmenite and rutile). Quartz in the sinter is a residual phase from the rock fragment (*i.e.* quartz in the sinter is not diagenetic).

https://doi.org/10.1346/CCMN.2007.0550208 Published online by Cambridge University Press

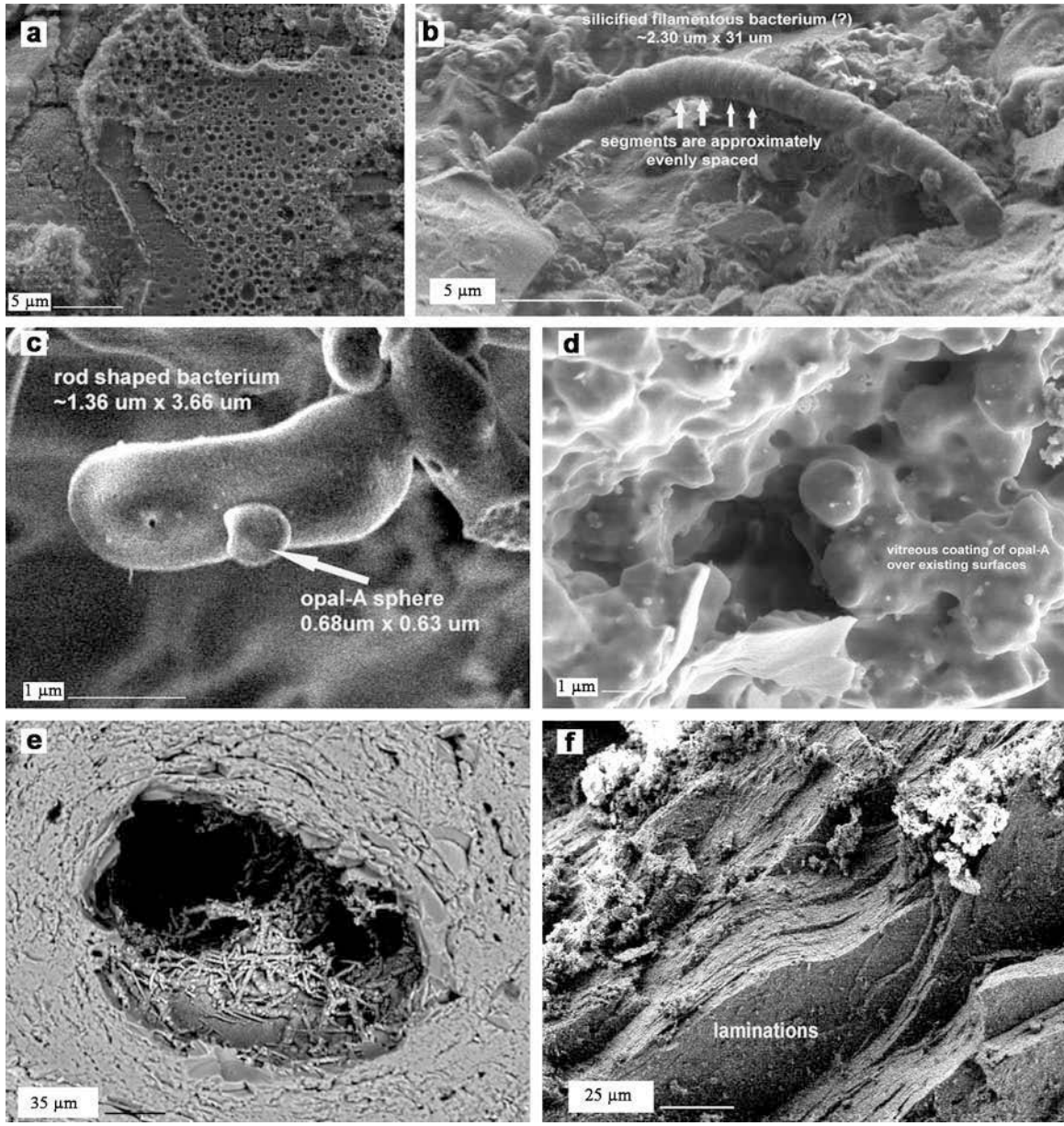

Figure 8. SEM images from each zone of the sinter. Image a is from the crustal zone, b and c from the altered zone, d from the dark/light laminated zone, and e and f from the dark laminated zone. (a) honey-comb textured sinter, (b) segmented filament, (c) opal-A sphere and rod-shaped structure attached to substrate, (d) vitreous opal-A coating, (e) BSE image of pore space embedded with filamentous structures resembling microorganisms, and (f) laminations found in the dark zone.

Strong evidence to support the idea that the altered zone was a volcanic rock is the presence of pseudobrookite ($Fe^{3+}_{1.5}Fe^{2+}_{0.4}Mg_{0.1}Ti_{0.75}Fe^{2+}_{0.25}O_5$). This mineral has been documented in only a few places in the United States, such as the Thomas Range, Utah and Sierra County, New Mexico (Foord *et al.*, 1995), and found to occur in association with rhyolitic cavities. Given the known localities of pseudobrookite, it is believed that this mineral was not deposited by aeolian forces. Pseudobrookite and its alteration products form by the following reaction:

$$2FeTiO_3 + O_2 \rightarrow Fe_2TiO_5 \rightarrow Fe_2O_3 + TiO_2 \quad (1)$$

Ilmenite oxidizes to pseudobrookite then breaks down to form hematite and rutile. Given that only one sinter deposit was analyzed in this study, additional sinter sample analysis is required to determine if clay formation is due to isolated events or if it is commonly found in sinters along the vent rim of Octopus Spring.

The influence of clays on the silicification process occurs in two stages. The first involves the alteration phase of the pre-existing rhyolitic rock fragment. The

https://doi.org/10.1346/CCMN.2007.0550208 Published online by Cambridge University Press

geochemical effects of this process can be idealized by reaction between albite and smectite, which is written as,

$$\underset{\text{plagioclase in rhyolite}}{1.8NaAlSi_3O_8} + \underset{\text{acid}}{1.2H^+} \rightarrow \underset{\text{smectite}}{Na_{0.4}Al_{1.8}Si_4O_{10}(OH)_2} + \underset{\text{silica}}{1.4H_4SiO_4^0} + \underset{\text{ions}}{1.2Na^+} \quad (2)$$

This first-step reaction has the effect of locally raising pH and dissolved silica, which promotes the precipitation of opal-A. Ca-bearing groundwater derived from plagioclase dissolution and mixing with spring fluids may contribute towards trace calcite precipitation within the sinter. Once the rhyolitic rock fragment has reacted and calcite has precipitated, pH and dissolved silica concentration would be expected to be reduced locally. During this step (*i.e.* in the absence of additional smectite formation and with time and temperature), initially formed opal-A would be expected to dehydrate and dissolve with silica re-precipitating as opal-CT, opal-C and/or opal-T. The honeycomb structure in Figure 8a is interpreted to have formed as opal-A spheres dissolved back into solution. The radial crack features observed in the laminated region of the sinter are consistent with the dehydration step of the opal-A transformation; however, the presence of smectite should have an inhibitory effect on the opal-CT formation as discussed above. The absence of opal-CT in the older interior regions of the sinter and presence of opal-A/CT in the younger spicular region indicates that the smectite probably has an inhibitory effect on the transformation of opal-A.

Role of smectite in microbial preservation

The presence of smectite may influence primary microbial silicification. The formation of smectite from feldspar produces excess silica that is released into surrounding fluids, thus increasing local silica concentrations. This increase in silica would increase the rate of microbial cells undergoing extracellular silicification, given that microbial cells often act as templates for silica formation in terrestrial hot-spring systems. Once the feldspar has completely hydrolyzed, smectite formation no longer contributes to the silicified microbial cells (unless it was dissolved to form halloysite). A detailed analysis that compares sinter deposits with and without smectite forming under the same physiological conditions as terrestrial hot springs would add new insights, which would help resolve the exact role of smectite in microbial silicification. Until both conditions can be carefully examined, we can only suggest smectite formation as a potential mechanism to influence microbial silicification.

The silicification of microbial life has been well documented within hot-spring systems where sinters are activity forming (Schultze-Lam *et al.*, 1995; Cady and Farmer, 1996; Renaut *et al.*, 1998; Jones *et al.*, 2001). Two mechanisms have been proposed for how silica binds to the surface of a bacterial cell, both involving the interaction of ions dissolved in spring fluids and the microbial cell wall. The first is direct contact between the dissolved silica in solution and the microbial cell wall (see Mera and Beveridge, 1993; Westall *et al.*, 1995), and the second involves the formation of a metal ion bridge between the cell wall and silica in solution (Fortin and Beveridge, 2000; Mera and Beveridge, 1993). As the interaction between the cell surface and ions in solution persists, silica will continue to form around the microbes, entombing the microbe over time, leaving behind a silicified tube as the only textural signature of the microbes' existence. The siliceous filamentous structures noted through SEM (Figure 8b,e) are believed to be silicified microorganisms due to the morphological resemblance. The silicified structure that is found in the clay-dominant region of the sinter contains evenly spaced segments resembling septa found in microorganisms (Figure 8b) known to exist in Octopus Spring (Blank *et al.*, 2002). It is unlikely that these segments resulted from opal-A spheres cementing together, as opal spheres tend to elongate into large spherical structures (Westall *et al.*, 1995).

In addition to microbial morphological signatures, microorganisms can leave a chemical signature within the rock record. Examination of the C/N ratios for each region shows that the altered smectite-bearing zone contains a greater proportion of C. Both the C and N are retained after heating to 450ºC and are operationally defined as fixed N and fixed C. Fixed N is most commonly found in the form of NH_4^+ within mineral structures (Schroeder and Ingall, 1994) and fixed C in carbonates. The fixed C/N ratios observed in this study are not carbonate free, and are therefore less than that of typical plant material at 15:1 (Brooks *et al.*, 2003). The C/N values range from 8:1 to 15:1 for microbes found in a surface horizon of a terrestrial soil (Demas and Rabenhorst, 1999). Soil samples collected from Te Kopia geothermal fields over a temperature range of 15–90ºC and at pH range of 3.7–4.6 show average C/N values of 25:1 (Burns, 1997). The bulk C/N ratios in the sinter are within the range of soil microbes, lending further credence to the idea that the biological signatures are becoming incorporated into the sinter.

Fixed C contributes to the total C in the form of calcite, which exists as a trace phase in most zones. This calcite forms as dissolved Ca increases with plagioclase breakdown in combination with increased pH during hydrolysis. Occlusion of calcite by co-precipitating opal-A aids the preservation of calcite which can potentially dissolve at lower pH levels as the hydrolysis reaction with feldspar stops.

The large buffering capacity and large cation exchange capacity of smectites have been shown to stimulate microbial respiration in a variety of soil bacteria, through maintaining near-neutral pH for cell

https://doi.org/10.1346/CCMN.2007.0550208 Published online by Cambridge University Press

growth (Stotzky and Rem, 1966; Stotzky, 1966). Montmorillonites were shown to shorten the lag time of microbial growth (Stotzky and Rem, 1966), therefore establishing the exponential growth phase at increased rates where growth and cell division is at its maximum rate. If microorganisms are living within the pore spaces and/or along the edges of the smectite-dominated zones, then respiring micoorganisms may be taking advantage of the redox properties of these clays (*i.e.* lithotrophic reaction of $Fe^{2+} \rightarrow Fe^{3+}$ in octahedral sites). Also, the fixed N in the altered zone is possibly a result of microbial activity where NH_3 excreted by microorganisms protonates to NH_4^+. Ammonium values of <0.04 mg/L have been detected within Octopus Spring (McCleskey *et al.*, 2004). This N can become incorporated into the interlayer of smectite (Ransom *et al.*, 1999) providing a nitrogen signature for microbial life within the clays. The greater microbial respiration rate and increase in cell numbers caused by the presence of smectite during this time frame would increase the likelihood of N becoming incorporated into smectite. Ammonification of amino acids from a lysed bacterial cell could also participate in the nitrogen signature held in these clays. An abiotic source of fixed N could also result from N_2 reduction from the atmosphere by ferrous Fe within the rock, such as the pseudobrookite redox (reaction 1). Large biogenic NH_4^+ values from hot-springs fluids within the Uzon Caldera, Kamchatka, Russia (Schroeder *et al.*, 2006) have been recorded using N isotopes; stable isotope work was beyond the scope of the present study.

The onset of the opal-A to opal-CT phase change is inhibited in all regions of the sinter except in the spicular region due to the porous nature of siliceous sinters. Although smectites delay opal-CT formation, the prolonged preservation of silicified microbial forms would not occur as opal-A continues to dissolve into solution (shown by the honeycomb texture) and undergoes maturation at a rate expected without the presence of smectite. Despite the inability for prolonged morphological preservation, smectitic clays have the potential to preserve a microbial chemical signature as fixed N that is retained with smectite structure, and also the initial formation of smectitic clays may cause an increase in microbial silicification as excess silica is released.

CONCLUSIONS

Detailed study of a siliceous sinter from Octopus Spring in YNP indicates that the alteration of rhyolitic rock into smectite has affected the opal-A to opal-CT phase change. The presence of smectitic clay minerals during opal-A formation inhibits opal-CT formation. Although the exact mechanism for this inhibition is not known in terrestrial hot springs, the mechanism of Mg ion-site competition, which is known to catalyze nucleation sites for opal-CT growth in sedimentary basins appears to be a plausible causative factor (Kastner *et al.*, 1977). The onset of opal-CT was only found in the spicular region, which is unexpected given that the region represents the newest growth of the sinter deposit. Within this sinter, an interior altered region exists that is dominated by dioctahedral smectite and quartz with trace amounts of pseudobrookite, ilmenite, rutile and hematite. The altered zone is the site of Fe redox reaction, which may serve to facilitate microbe metabolism. The clay-rich altered zone retains the greatest amount of fixed N (operationally defined as N retained upon combustion at 450ºC). The fixed N represents ammonium trapped in the exchangeable interlayer site of the smectite. This N has the potential to serve as a biological signature of microbial activity in ancient hydrothermal systems.

ACKNOWLEDGMENTS

This work was supported by grants from the National Science Foundation's Biocomplexity in the Environmental Coupled Biogeochemistry Cycles Program (EAR-BE-0221905) and Microbial Observatories Program (NSF-MCB-0238407). The sample was collected through the Department of Interior National Park Service permit YELL-2002-SCI-1800. We would like to thank Juergen Wiegel for the opportunity to collect the sample, Chris Fleisher for his help in collecting data with the electron microprobe, Dr John Shields for his assistance with the SEM, Chris Romanek for the TGA analysis, and the comments of Sherry Cady. The reviews of Jessica Elzea-Kogel and Tetsuchi Takagi improved the manuscript.

REFERENCES

Bailey, S.W. (1984) Classification and structures of the micas. Pp. 1–12 in: *Micas* (S.W. Bailey, editor). Reviews in Mineralogy, **13**, Mineralogical Society of America, Washington, D.C.

Ball, J.W., Nordstrom, D.K., Jenne, E.A. and Vivit, D.V. (1998) Chemical analyses of hot springs, pools, geysers, and surface water from Yellowstone National Park, Wyoming, and vicinity, 1974–1975, *US Geological Survey Open-file Report*, 98-182, 45 pp.

Barger, K.E. and Beeson, M.H. (1981) Hydrothermal alteration in research drill hole Y-2, Lower Geyser Basin, Yellowstone National Park, Wyoming. *American Mineralogist*, **66**, 473–490.

Blank, C.E., Cady, S.L. and Pace, N.R. (2002) Microbial composition of near-boiling silica-deposition thermal springs throughout Yellowstone National Park. *Applied and Environmental Microbiology*, **68**, 5123–5135.

Braunstein, D. and Lowe, D.R. (2001) Relationship between spring and geyser activity and the deposition and morphology of high temperature (> 73ºC) siliceous sinter, Yellowstone National Park, Wyoming, U.S.A. *Journal of Sedimentary Research*, **71**, 747–763.

Brooks, P.D., Geilmann, H., Werner, R.A. and Brand, N.A. (2003) Letter to the editor. *Rapid Communications in Mass Spectroscopy*, **17**, 1924–1926.

Burns, B. (1997) Vegetation change along a geothermal stress gradient at the Te Kopia steam field. *Journal of Soil Royal Society of New Zealand*, **27**, 279–94.

Cady S.L. and Farmer, J.D. (1996) Fossilization processes in siliceous thermal springs: trends in preservation along thermal gradients. Pp. 150–173 in: *Evolution of*

Hydrothermal Ecosystems of Earth (and Mars?). Wiley, Chichester, UK (Ciba Foundation Symposium 202).

Demas, G.P. and Rabenhorst, M.A. (1999) Subaqueous soils: Pedogenesis in a submersed Environment. *Soil Science Society of America Journal*, **63**, 1250–1257.

Foord, E.E, Ayuro, R.A., Hoover, D.B. and Klein, D.P. (1995) Preliminary compilation of descriptive geoenvironmental mineral deposit models. *USGS Open-File Report* 95-831.

Fortin, D. and Beveridge, T.J. (2000) Mechanistic routes towards biomineral surface development. Pp. 7–24 in: *Biomineralization: From Biology to Biotechnology and Medical Application* (E. Baeuerlein, editor). Wiley-VCH, Verlag, Germany.

Founier, R.O. and Rowe, J.J. (1966) Estimation of underground temperatures from the silica content of water from hot springs and steam wells. *American Journal of Science*, **264**, 685–697.

Fritz,W.J. (1985) *Roadside Geology of the Yellowstone country*. Mountain Press, Missoula, Missouri, UK.

Guggenheim, S. and Kostner van Groos, A.F. (2001) Baseline studies of The Clay Minerals Society Source Clays: thermal analysis. *Clay and Clay Minerals*, **49**, 433–443.

Herdianita, N.R., Rodgers, K.A. and Browne, P.L. (2000) Routine instrumental procedures to characterize the mineralogy of modern and ancient silica sinters. *Geothermics*, **29**, 65–81.

Hinman, N.W. and Lindstrom, R.F. (1996) Seasonal changes in silica deposition in hot spring systems. *Chemical Geology*, **132,** 237–246.

Isaacs, C.M. (1982) Influence of rock composition on kinetics of silica phase changes in the Monterey Formation, Santa Barbara area, California. *Geology*, **10**, 304–308.

Jones, B., Renaut, R.W. and Rosen, M.R. (2001) Taphonomy of silicified filamentous microbes in modern geothermal sinters – implications for identification. *Palaios*, **16**, 580–592.

Jones, B., Renaut, R.W. and Rosen, M.R. (2003) Silicified microbes in a geyser mound: the enigma of low-temperature cyanobacteria in a high-temperature setting. *Palaios*, **18**, 87–109.

Kastner, M., Keene, J. and Gieskes, J. (1977) Diagenesis of siliceous oozes – I. Chemical controls on the rate of opal-A to opal-CT transformations – an experimental study. *Geochimica et Cosmochimica Acta*, **41**, 1041–1059.

Konhauser, K.O., Jones, B., Reysenbach, A. and Renaut, R.W. (2003) Hot spring sinters: keys to understanding Earth's earliest life forms. *Canadian Journal of Earth Science*, **40**, 1713–1724.

Konhauser, K.O., Jones, B., Phoenix, V.R., Ferris, G. and Renaut, R.W. (2004) The microbial role in hot spring silicification. *Ambio*, **33**, 552–558.

Lowe, D.R. and Braunstein, D. (2003) Microstructure of high-temperature (>73ºC) siliceous sinter deposited around hot springs and geysers, Yellowstone National Park: the role of biological and abiological processes in sedimentation. *Canadian Journal of Earth Science*, **40**, 1611–1642.

Lynne, B.Y. and Campbell, K.A. (2004) Morphologic and mineralogic transitions from opal-A to opal-CT in low-temperature siliceous sinter diagenesis, Taupo Volcanic Zone, New Zealand. *Journal of Sedimentary Research*, **74,** 561–579.

Lynne, B.Y., Campbell, K.A., Perry, R.S., Browne, P.R.L. and Moore, J.N. (2006) Acceleration of sinter diagenesis in an active fumerole, Taupo volcanic zone, New Zealand. *Geology*, **34** 749–752.

MacEwan, D.M.C. and Wilson, M.J. (1980) X-ray diffraction procedures from clay mineral identification. Pp. 305–360 in: *Crystal Structures of Clay Minerals and their X-ray Identification* (G.W. Brindley and G. Brown, editors). Monograph **5**, Mineralogical Society, London.

McCleskey, R.B., Ball, J.W., Nordstrom, D.K., Holloway, J.M. and Taylor, H.E. (2004) Water-chemistry data for selected hot springs, geysers, and streams in Yellowstone National Park, Wyoming, 2001–2002, *U.S. Geological Survey Open-file Report*, 2004-1316, 94 pp.

Mera, M.U. and Beveridge, T.J. (1993) Mechanism of silicate binding to the bacterial cell wall in *Bacillus subtilis*. *Journal of Bacteriology*, **175**, 1936–1945.

Moore, D.E. and Reynolds, R.C. (1997) *X-ray Diffraction and the Identification and Analysis of Clay Minerals*, 2nd edition. Oxford University Press, New York.

Murata, K.J. and Larson, R.R. (1975) Diagenesis of Miocene siliceous shales, Temblor Range, California. *Journal of Research US Geological Survey*, **3**, 553–556.

Pancost, R.D., Pressley, S., Coleman, J.M., Benning, L.G. and Mountain, B.W. (2005) Lipid biomolecules in silica sinters: indicators of microbial biodiversity. *Environmental Microbiology*, **7**, 66–77.

Ransom, B., Bennett, R.H., Baerwald, R., Hulbert, M.H. and Burkett, P.J. (1999) In situ conditions and interactions between microbes and minerals in fine-grained marine sediments: A TEM microfabric perspective. *American Mineralogist*, **84**, 183–192.

Renaut, R.W., Jones, B. and Tiercelin, J.J. (1998) Rapid *in situ* silicification of microbes at Loburu hot springs, Lake Bogoria, Kenya Rift Valley. *Sedimentology*, **45**, 1083–1103.

Reynolds, R.C. (1980) Interstratified clay minerals. Pp. 249–303 in: *Crystal Structures of Clay Minerals and their X-ray Identification* (G.W. Brindley and G. Brown, editors). Monograph 5, Mineralogical Society, London.

Rice, S.B., Freud, H., Huang, W.L., Clouse, J.A. and Isaacs, C.M. (1995) Applications of Fourier transform infrared spectroscopy to silica diagenesis: The opal-A to opal-CT transformation. *Journal of Sedimentary Research*, **65**, 639–647.

Rimstidt, J.D. and Cole, D.R. (1983) Geothermal mineralization I: The mechanism of formation of the Beowawe, Nevada, siliceous sinter deposit. *American Journal of Science*, **283,** 861–875.

Schroeder, P.A. and Ingall, E.D. (1994) A method for the determination of nitrogen in clays, with application to the burial diagenesis of shales. *Journal of Sedimentary Research*, **A64**, 694–697.

Schroeder, P.A. and McLain, A.A. (1998) Illite-smectites and the influence of burial diagenesis on the geochemical cycling of nitrogen. *Clay Minerals*, **33**, 539–546.

Schroeder, P.A., Cady, S, Crowe, D.E., Karpov, G., King, G., Mills, G., Neal, A., Bonch-Osmosolovskaya, E., Robb, F., Romanek, C., Sokolova, T., Wiegel, J. and Zhang, C. (2006) *Geothermal Biology and Geochemistry in Kamchatka, Russia: Connections between Uzon Caldera, Geyser Valley and the YNP - Research Coordination Network*. NSF-sponsored Research Coordination Network workshop and Thermal Biology Institute, Montana State University. Abstract with program, www.rcn.montana.edu.

Schultze-Lam, S., Ferris, F.G., Konhauser, K.O. and Wiese, R.G. (1995) In situ silicification of an Icelandic hot spring microbial mat: implications for microfossil formation. *Canadian Journal of Earth Sciences*, **32**, 2021–2026.

Stotzky, G. (1966) Influence of clay minerals on microorganisms III. Effect of particle size, cation exchange capacity, and surface area on bacteria. *Canadian Journal of Microbiology*. **12**, 1235–1246.

Stotzky, G. and Rem, L.T. (1966) Influence of clay minerals on microorganisms I. Montmorillonite and kaolinite on bacteria. *Canadian Journal of Microbiology*, **12**, 547–563.

Westall, F., Boni, L. and Guerzoni, E. (1995) The experimental

silicification of microorganisms. *Palaeontology*, **38**, 495–528.

Yoshito, N. (2002) Diffusion of H_2O and I^- in expandable mica and montmorillonite gels: Contribution of bound H_2O. *Clays and Clay Minerals*, **50**, 1–10.

(*Received January 2006; revised 8 November 2006; Ms. 1134; A.E. Warren D. Huff*)